

Polarization-controlled Plasmonic Structured Illumination

Qilong Tan,^{†,‡} Zhengji Xu,^{‡,‡,} Dao-Hua Zhang,[‡] Ting Yu,[§] Shuang Zhang,^{†,*} and Yu Luo,^{§,*}*

[†]School of Physics & Astronomy, University of Birmingham, Birmingham, Edgbaston, B15

2TT, United Kingdom

[‡]Institute of Microelectronics, Agency for Science, Technology and Research (A*STAR),

138634, Singapore

[‡]School of Electrical & Electronic Engineering, Nanyang Technological University, 639798,

Singapore

[§]School of Physical and Mathematical Sciences, Nanyang Technological University, 637371,

Singapore

Abstract: Structured light in the subwavelength scale is important for a broad range of applications ranging from lithography to imaging. Of particular importance is the ability to dynamically shift the pattern of the fields, which has led to the development of structured illumination microscopy. Further extension of structured illumination to plasmonic systems has enabled imaging beyond diffraction limit. However, structured illumination usually requires complicated optical setups

entailing moving mechanical parts. Here a polarization tunable structured plasmonic fields (SPF) is proposed and experimentally demonstrated. The SPF is formed by surface plasmon interference (SPI) generated by a fishbone-shaped metasurface on a thin gold film. Importantly, the SPF can be continuously shifted by merely varying the linear polarization state of an incident beam. The precise control of the fringes of structured illumination and elimination of mechanical control will have great potential in subdiffractional imaging for practical applications.

KEYWORDS: Plasmonic, metasurface, structured illumination, subdiffractional imaging

Plasmonics is providing a powerful means for manipulating light in the subwavelength regime. At the interface between a metal and a dielectric, the collective oscillation of the free electrons can support surface mode which can have a wavelength much less than that of the free space radiation.¹ Structured metallic surfaces have attracted growing interest since they can be designed to couple free space illumination into surface plasmon polaritons (SPPs) and to further manipulate the propagation of SPPs². This has formed the basis for a plethora of interesting phenomena such as extraordinary optical transmission (EOT) and applications such as lithography, super-imaging³⁻⁶.

In recent years, plasmonic structures in the nanometer scale have been used as the building blocks to construct metasurfaces for controlling the wavefront, polarization state and intensity of light in a way that goes beyond the conventional optics⁷. Various applications have been implemented with metasurfaces, such as metalenses⁸⁻¹⁰, computer generated holography¹¹⁻¹³,

unidirectional excitation of SPPs ^{2,14-16} etc. Interestingly, metasurfaces can be designed to exhibit switchable optical functionalities controlled by the polarization state of the incident light. In particular, the scattering phase of each constituent element of metasurfaces can be made polarization-dependent via two means: resonance induced dynamic phase and orientation-controlled geometric phase. The former allows for independent and arbitrary phase profiles on each of the two orthogonal linear polarizations ^{7,17-20}. The latter, i.e. geometric phase approach, allows for precise and spin-dependent control of the phase profiles ²¹⁻²⁴. Polarization-dependent phase utilizing either dynamic or geometric phase designs alone is limited to switching between two states, while combining dynamic and geometric phase can provide extra degrees of freedom for phase modulation, which has led to a number of applications including generation of polarization-independent orbital angular momentum ²⁵, phase control of arbitrary orthogonal states ²⁶.

In this paper, we experimentally demonstrate dynamically controllable plasmonic fringe patterns formed by two counter propagating surface plasmon beams. The shift of periodic SPI can be accurately tuned by simply rotating the direction of incident linear polarization. Based on this scheme, a practical application of SIM is proposed and numerically simulated utilizing the polarization-controlled tunable structured SPI. In contrast, the shifts of structured SPI in previous works were tuned by varying the excitation angle ^{4,6,27} or wavefront of incident light ²⁸, entailing complicated mechanical device or costly optical components, such as Galvo scanner, digital micromirror device and high NA. objective. Our approach eliminates the need for mechanical

moving parts and may provide potential practical applications such as structured illumination microscopy (SIM)²⁹⁻³¹, maskless lithography,^{32,33} and optical manipulation³⁴.

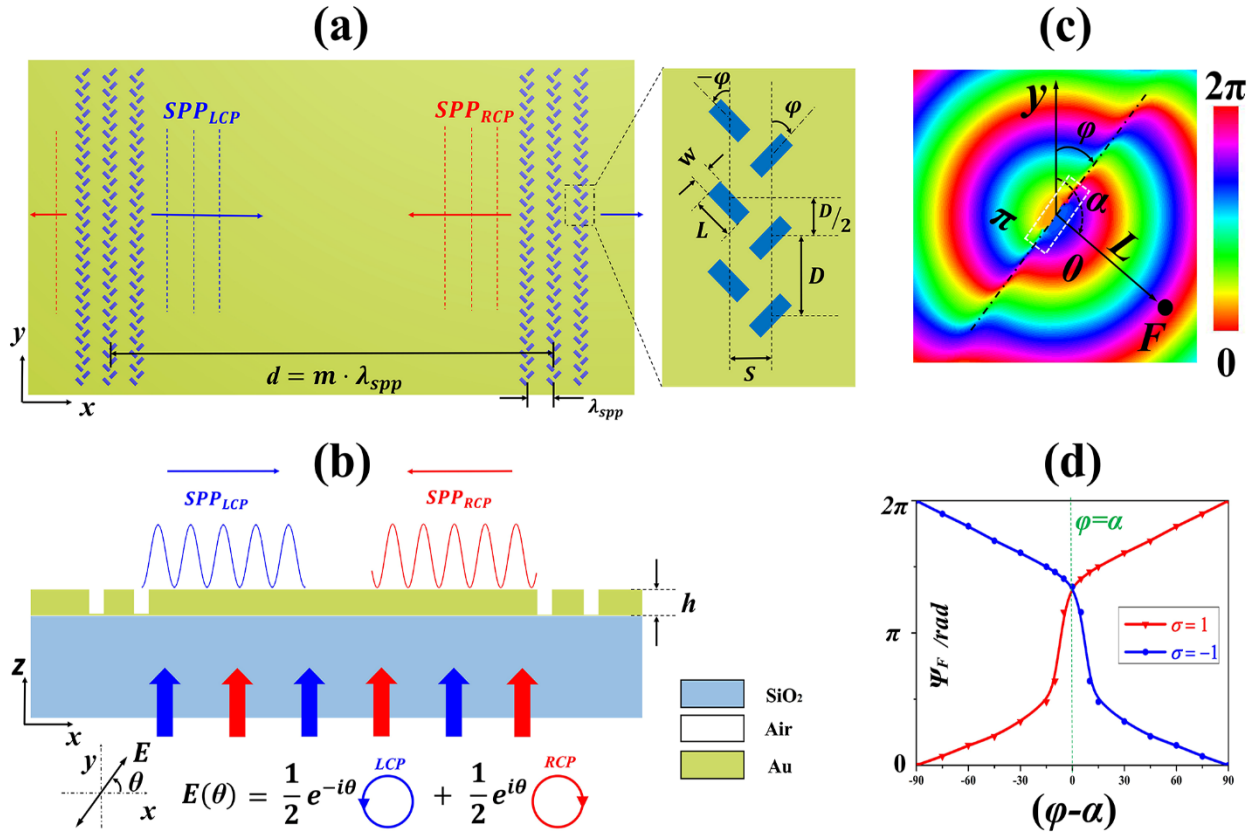


Figure 1. Schematic of generated polarization controlled tunable SPI. (a) The fishbone grating array of nano apertures on a gold film excites SPI on the gold/dielectric surface. (b) SPPs excited by RCP and LCP components interfere in the defect between two adjacent grating arrays. (c) The phase distribution of the SPPs excited by a single nano aperture. It shows an anti-phase pattern relative to the long axis of nano aperture. (d) The relation between phase of SPPs and the orientation angle at a view point $F(\alpha, L)$.

In order to achieve polarization controlled tunable SPI, we employ periodic fishbone grating arrays carved in a thin gold film as shown in Figure 1a. Fishbone grating array has been utilized to realize tunable unidirectional excitation of SPPs by different circularly polarized beams^{2, 14}. Each unit cell contains two orthogonal nanoslits separated in both x and y directions, with their orientations forming an angle φ of $-\pi/4$ and $\pi/4$ respectively with the y axis. Each single anisotropic nano-aperture can be approximately regarded as a local subwavelength dipole antenna, with its orientation perpendicular to the long axis of nano aperture. The SPPs pattern excited from a nano aperture is approximately that of an in-plane point dipole and exhibits an anti-phase radiation pattern (Figure 1c) about the long axis of nano aperture. Under the illumination of a circularly polarized beam with spin σ , where $\sigma = \pm 1$ represent the right-handed and left-handed polarization states, respectively, each dipole moment acquires a geometric phase $\sigma\varphi$. Therefore, the spin dependent phase of the SPPs excited by each aperture can be obtained by varying the orientation angle φ of the nano-aperture. When the nanoslits are arranged in an array in the y direction with lattice constant less than the SPP wavelength (Figure 1a), the SPP can only be excited in the +x and -x directions. The SPPs excited by the two columns of apertures can be expressed as:

$$E_{spp}(x) = |E_1| e^{-i[k_{spp}(x+Sv)+\sigma\pi/4]} + |E_2| e^{-i(k_{spp}x-\sigma\pi/4)} \quad (1)$$

where $|E_1|$ and $|E_2|$ are the amplitude of SPPs excited by the two columns of apertures, respectively, with $|E_1| = |E_2|$, $v = \pm 1$ represents the SPP wave excited along the +x and -x direction, respectively. k_{spp} is the magnitude of SPPs wave vector, which can be expressed as:

$$k_{spp} = \frac{\omega}{c} \sqrt{\frac{Re(\varepsilon_m) \cdot \varepsilon_d}{Re(\varepsilon_m) + \varepsilon_d}} \quad (2)$$

where ω and c represent the circular frequency and the velocity of light in vacuum, ε_m and ε_d are the permittivities of the gold and dielectric, respectively. The intensity of SPPs excited by each pair of columns of apertures can be expressed as:

$$|E_{spp}|^2 = |E_1|^2 \left[1 + e^{-i(k_{spp}Sv + \sigma\pi/2)} \right]^2 \quad (3)$$

From Eq. 3, when $S = \lambda_{spp}/4$, SPPs are only excited to the right or left direction by an incident light of spin state $\sigma = -1$ or $+1$, respectively, leading to tunable unidirectional SPPs controlled by the circular polarization states of the incident light.

For a linearly polarized incident beam, it can be decomposed into left circular polarization (LCP) and right circular polarization (RCP) components with a $e^{i2\theta}$ phase difference between them. Hence the metasurface can excite SPPs along both $+x$ and $-x$ directions, with each one generated by a particular circular component of the incident beam respectively. Hence there is a phase difference of 2θ between the left and right going SPPs. The SPPs excited by LCP/RCP component can be respectively expressed as:

$$SPP_{LCP} = E_L \cdot e^{i(\omega t - k_{spp} \cdot x - \theta)} \quad (4)$$

$$SPP_{RCP} = E_R \cdot e^{i(\omega t + k_{spp} \cdot x + \theta + \pi)} \quad (5)$$

where E_L and E_R are the amplitude of SPPs excited by different circular components of the incident beam, respectively, and $E_L = E_R$. The extra phase π in Eq. 5 arises from anti-symmetric phase distribution of the radiation pattern of individual apertures along x and $-x$ directions as shown in

Figure. 1c. When two metasurfaces of finite width are positioned a certain distance away from each other, there would be interference patterns in the unpatterned region sandwiched between the two metasurfaces under linear polarization illumination, as shown in Figure 1b. Specifically, the interference is formed by the left-going SPPs launched from the metasurface located on the right side, excited by the LCP component of the incident beam, and the right-going SPPs launched from the metasurface located on the left side, excited by the RCP component. By continuously tuning the metasurface located on the left side, excited by the RCP component. By continuously tuning the linear polarization angle θ of the incident beam, the relative phase of the left-going and right-going SPPs are varied as 2θ . The interference fringe of SPPs excited by the two components can therefore be expressed as:

$$I_{SPP} = |SPP_{LCP} + SPP_{RCP}|^2 = 2E_L^2 [1 - \cos 2(k_{SPP}x + \theta)] \quad (6)$$

Thus, the sinusoidal fringe formed by SPI can be continuously shifted by rotating the direction of linear polarization.

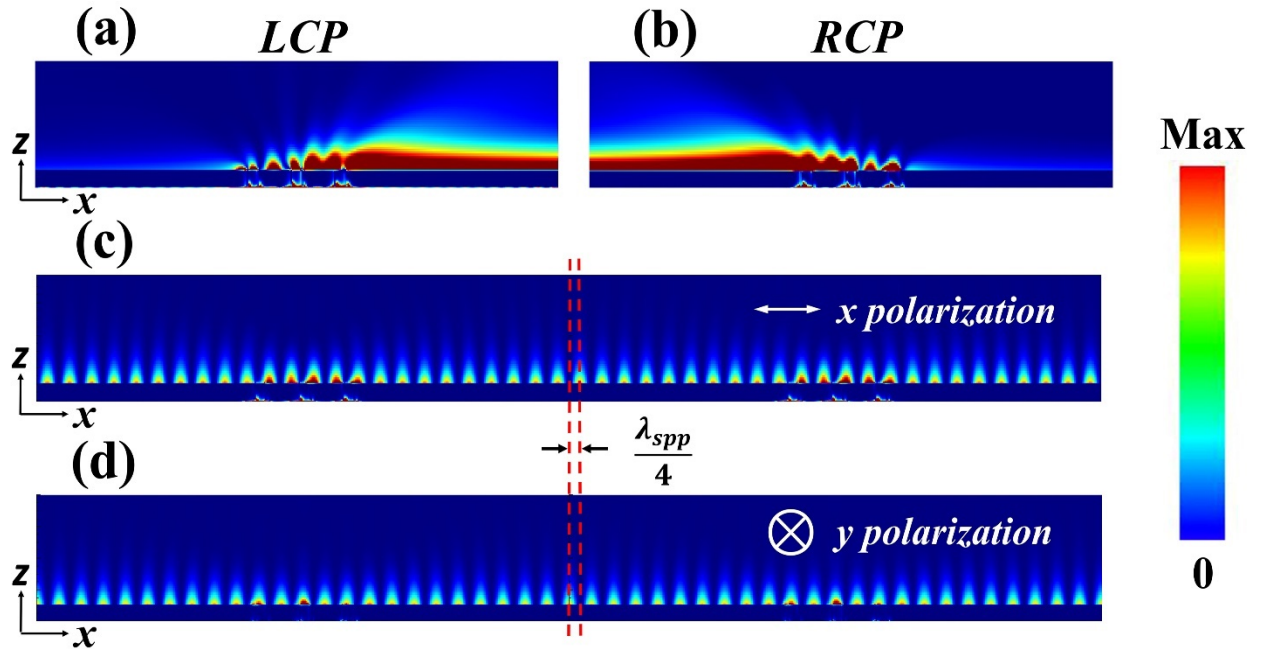


Figure 2. Numerical demonstrations of polarization tunable structured illumination. The fishbone grating array launch tunable unidirectional SPP by LCP (a) and RCP. (b). Unidirectional launching SPPs excited by two groups of fishbone grating array form interference fringe. The intensity distribution of SPI excited by x (c) and y (d) polarization.

To demonstrate the polarization-controlled structured illumination described above, we fabricate fishbone grating arrays on a gold film with the following parameters: $w=90nm$, $L=180nm$, $S=152nm$, $D=300nm$, $h=210nm$, $d=7.3\mu m$ and $\phi=\pi/4$ working at $\lambda=632.8nm$. The wavelength of SPPs on the gold/air interface is $\lambda_{spp}=608nm$. There is a vertical offset between neighboring columns of apertures to reduce the near-field coupling between adjacent columns of nano-apertures. A relatively thick gold film ($h=210nm$) is used to block direct transmission of light.

As shown in Figure 2a, b, our FDTD simulation shows that the metasurface structure designed above can launch spin-dependent unidirectional SPPs when excited by a circularly polarized incident beam. For linearly polarized incident beams, between the two fishbone grating arrays, the SPPs excited by two gratings interfere and form the interference fringe. The intensity distribution of SPI excited by x and y polarization are showed in Figure 2c, d. The red dash lines mark the position with maximum of SPI for x and y polarization, respectively. It is observed that the interference fringe laterally shifts $\lambda_{spp}/4$ between the two linear polarization states of the incident beam. Further FDTD simulation shows that the position of the fringe can be continuously shifted

by gradually rotating incident linear polarization, which agrees well with the theoretical prediction based on Eq. 6.

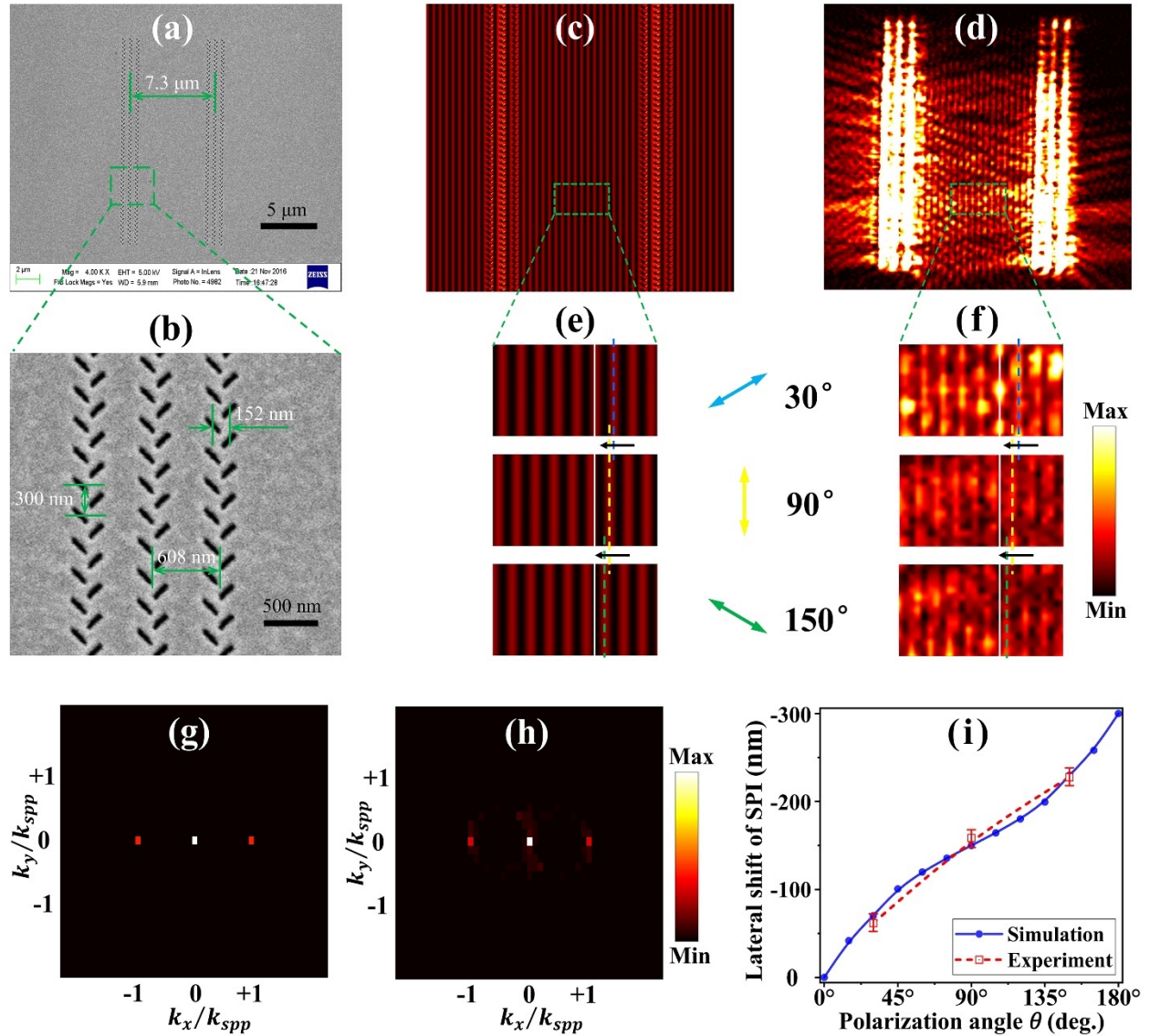


Figure 3. Experimental characterization of polarization tunable structured illumination. (a) Scanning electron microscope (SEM) image of gold film with periodic fishbone grating arrays. (b) Further magnified view of (a). The simulated (c) and experimental (d) intensity distribution of SPI are detected 10 nm above the gold/air interface under 30° polarized incidence. Local intensity

distribution of SPI under different polarization angles by simulation (e) and experiment (f), respectively. Fourier transforms of the simulated (g) and experimental (h) SPI. (i) Simulated and experimental lateral shift with different linearly polarized beams.

To experimentally confirm the polarization-tunable plasmonic field fringe, we use the near-field scanning optical microscopy (NSOM) to characterize the SPPs intensity distributions. The light incidence from a He-Ne laser (Thorlabs, 0.5 mm beam width, 20 mW power, $\lambda=632.8$ nm) is TM polarized and focused onto the fishbone gratings from the bottom of the sample substrate at normal incidence by 10x objective lens (Olympus UPlanFLN NA=0.3). The NT-MDT NSOM system is mounted with an inverted microscope (Olympus IX71) equipped with a photomultiplier tube (PMT) for signal detection and amplification. The aluminum-coated NSOM probe tip is less than 100 nm in diameter and positioned approximately 10 nm from the sample substrate. The probe tip collects the near-field signal at a relatively stable distance. This distance is achieved by shear-force feedback mechanism to perform the precise control. The fiber tip is glued with a tuning fork, which is mounted on a piezoelectric tube dithering and scanning parallel to the sample surface. The vibration amplitude of the tuning fork changes rapidly as it approaches the sample surface perpendicularly at distances of about tens of nanometers. The resonance frequency is chosen as 33 KHz for quartz crystal tuning fork. The minimum scan distance of a step is 100 nm.

The gold film with periodic fishbone grating arrays is fabricated on the glass substrate using focused ion beam (FIB) from Carl Zeiss AURIGA crossbeam (FIB-SEM) workstation. The ion

source is Gallium (Ga) at 30keV beam energy. For milling the groove patterns, 20 pA beam current was chosen with minimum spot size of 13 nm. Its scanning electron microscope (SEM) images are shown in Figure 3a, b. Figure 3d shows the experimental SPPs intensity distribution under the normal incidence with 30° polarization, where the standing SPPs wave can be observed. The period of SPI detected is about 300 nm, which agrees well with the simulation. Figure 3f shows the field intensity distribution of SPPs in the same region under the excitations of a laser beam with different polarization angles (30°, 90° and 150°). The dash lines denote the position corresponding to the maximum of a SPI fringe. It is observed that the fringe laterally shifts at a step of about $\lambda_{spp}/6$ when the polarization angle is tuned from 30° to 150° at a step of 60°. The quality of measured interference fringe is limited by the scanning step, non-uniform illumination of incident beam and possible sample damages during the near-field scanning process. Via Fourier transform of the intensity distribution, the frequency contents of the interference fringe expressing in Eq. 6. can be expressed as:

$$I_{SPI}(k) = 2E_L^2 \left[\delta(k) - \frac{1}{2} \delta(k - k_{spp}) e^{-2i\theta} - \frac{1}{2} \delta(k + k_{spp}) e^{2i\theta} \right] \quad (7)$$

The first orders provide the information about the periodic SPI patterns. Thereinto, the lateral shift of the sinusoidal fringe tightly links with the phase shift of the +1 order $\Delta\phi$. And it can be more precisely calculated by $\lambda_{spp} \cdot \Delta\phi$. Figure 3g, h. show the Fourier transform of the simulated and experimental patterns, respectively. Both results reveal peaks at 0 and $\pm k_{spp}$, which is consistent with Eq. 7. Figure 3i shows the simulated and measured lateral shift of the fringe upon illumination of different linearly polarized beams. The plot shows that the lateral shift of the SPI

fringe can be continuously shifted by simply rotating the direction of incident linear polarization. However, we notice that the lateral shift is not strictly linear with the polarization of incident beams. This is caused by the unequal coupling efficiency of the fishbone grating between orthogonal linearly polarizations. The coupling efficiencies of the fishbone grating are calculated to be 1.1% and 3.4% for TE and TM polarized incident beam, respectively. This difference can be minimized by optimizing the structural parameters (see the Supporting Information for optimization details). The conversion efficiency can be further improved by optimizing the resonant properties of the nano apertures and by increasing the columns of the fishbone grating. Moreover, distance between the two patterned areas can be increased by reducing the attenuation of SPP. This may be achieved by using high quality metal films such as the single crystalline Au film^{35, 36}.

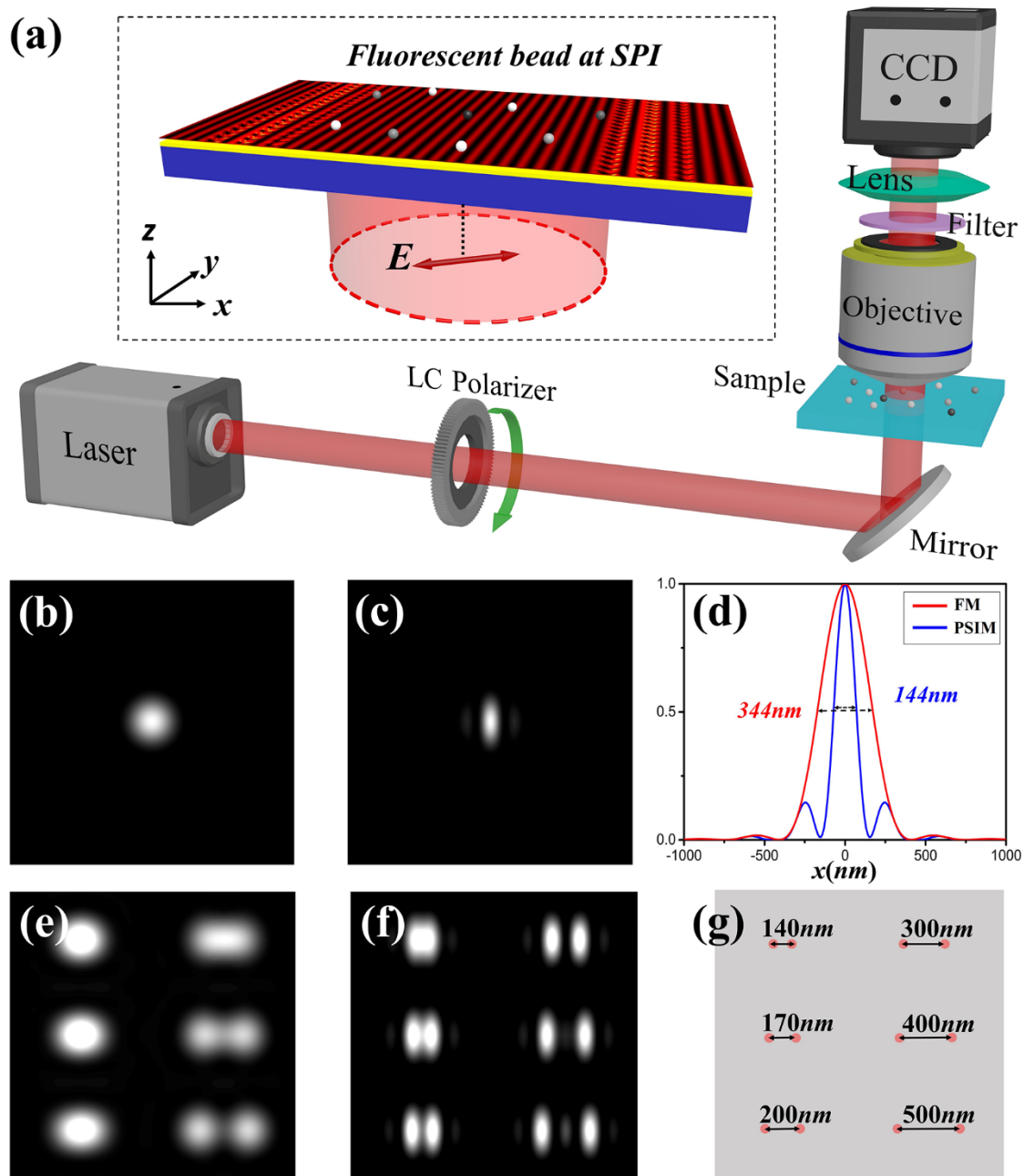


Figure 4. Simulation of PSIM resolution improvement. (a) Schematics of the PSIM system. The SPI will laterally shift by controlling the polarization angle through liquid crystal (LC) polarizer. (b-c) PSF of fluorescent microscope (FM) and PSIM, respectively. (d) The FWHM of PSF for x

direction. (e-f) Image of FM and PSIM for closely located fluorescent beads, respectively. (g) The corresponding distribution of fluorescent beads.

Finally, we discuss the imaging ability of the polarization-controlled SPI based on simulation. In the simulation, fluorescent beads with a diameter of 50 nm placed on top of a gold film are used as the objects to be imaged, as shown in the illustration of Figure 4a. The radiation wavelength of fluorescent beads (such as Fluorescent dye: CY5) is chosen as 670nm under the excitation of SPPs. In practice, the polarization angle of incidence can be rapidly and precisely manipulated by a liquid crystal (LC) polarizer. Employing a numerical reconstruction algorithm,^{4,31,37} the super-resolution image is reconstructed from three diffraction limited images under structured illumination of SPI formed by an incident laser beam with the linear polarizations 30°, 90° and 150° (see the Supporting Information for algorithm details). Compared with conventional FM (Figure 4b), the point spread function (PSF) of PSIM shown in Figure 4c is significantly compressed along x axis. The full width half maximum (FWHM) of PSF shown in Figure 5d are about 344nm and 144nm for FM and PSIM, respectively, representing a 2.3 fold resolution improvement. Figure 4 e-f shows the comparison of images between conventional FM and PSIM. The corresponding distribution of fluorescent beads is shown in Figure 4g, with the center to center distance of two adjacent fluorescent beads marked in the figure. Two closely located fluorescent beads, with lateral adjacent distance well below the diffraction limit can be distinguished utilizing the proposed structured illumination system.

In conclusion, we have demonstrated that polarization-controlled tunable phase profiles could be realized by utilizing the spin dependent unidirectional excitation of SPPs. The relationship between incident polarization state and phase of SPPs is studied both numerically utilizing FDTD simulation and experimentally using near field scanning. The phase-shifting of periodic SPI can be continuously tuned ranging from 0 to 2π by rotating the direction of incident linear polarization. Based on this, we evaluated the performance of a plasmonic SIM utilizing the polarization-controlled tunable SPI. Owing to the precise phase modulation of SPI without the need for mechanical control, the approach is promising a broad range of applications including super-resolution imaging, chemical analysis and maskless lithography.

ASSOCIATED CONTENT

Supporting Information

Optimization details of the fishbone grating and the reconstruction algorithm of PSIM. (PDF)

AUTHOR INFORMATION

Corresponding Authors

*E-mail: (Zhengji Xu.) xu_zhengji@ime.a-star.edu.sg

*E-mail: (Shuang Zhang) s.zhang@bham.ac.uk

*E-mail: (Yu Luo) luoyu@ntu.edu.sg

Author Contributions

[†] These authors contributed equally to this work.

Notes

The authors declare no competing financial interest.

ACKNOWLEDGMENT

This work is supported in part by Singapore Ministry of Education (Grants Tier 2 MOE2015-T2-1-145). SZ acknowledges financial support from H2020 European Research Council Project Nos. 734578 (D-SPA), 777714 (NOCTURNO) and 648783 (TOPOLOGICAL), the Royal Society and the Wolfson Foundation.

REFERENCES

- (1) Barnes, W. L.; Dereux, A.; Ebbesen, T. W. Surface plasmon subwavelength optics. *Nature* **2003**, 424(6950), 824-830.
- (2) Huang, L.; Chen, X.; Bai, B.; Tan, Q.; Jin, G.; Zentgraf, T.; Zhang, S. Helicity dependent directional surface plasmon polariton excitation using a metasurface with interfacial phase discontinuity. *Light: Science & Appl.* **2013**, 2(3), 70.
- (3) Liu, Z. W.; Wei, Q. H.; Zhang, X. Surface plasmon interference nanolithography. *Nano Lett.* **2005**, 5(5), 957-961.

(4) Wei, F.; Lu, D.; Shen, H.; Wan, W.; Ponsetto, J. L.; Huang, E.; Liu, Z. Wide field super-resolution surface imaging through plasmonic structured illumination microscopy. *Nano Lett.* **2014**, *14*(8), 4634-4639.

(5) Ma, Q.; Hu, H.; Huang, E.; Liu, Z. (2017). Super-resolution imaging by metamaterial-based compressive spatial-to-spectral transformation. *Nanoscale* **2017**, *9*(46), 18268-18274.

(6) Bezryadina, A.; Zhao, J.; Xia, Y.; Zhang, X.; Liu, Z. High spatiotemporal resolution imaging with localized plasmonic structured illumination microscopy. *ACS nano* **2018**, *12*(8), 8248-8254.

(7) Yu, N.; Genevet, P.; Kats, M.A.; Aieta, F.; Tetienne, J.P.; Capasso, F.; Gaburro, Z. Light propagation with phase discontinuities: generalized laws of reflection and refraction. *Science* **2011**, *334*(6054), 333-337.

(8) Chen, X.; Huang, L.; Mühlenbernd, H.; Li, G.; Bai, B.; Tan, Q.; Jin, G.; Qiu, C.; Zhang, S.; Zentgraf, T. Dual-polarity plasmonic metalens for visible light. *Nat. Commun.* **2012**, *3*, 1198.

(9) Aieta, F.; Genevet, P.; Kats, M. A.; Yu, N.; Blanchard, R.; Gaburro, Z.; Capasso, F. Aberration-free ultrathin flat lenses and axicons at telecom wavelengths based on plasmonic metasurfaces. *Nano Lett.* **2012**, *12*(9), 4932-4936.

(10) Chen, X.; Chen, M.; Mehmood, M. Q.; Wen, D.; Yue, F.; Qiu, C.; Zhang, S. Longitudinal multifoci metalens for circularly polarized light. *Adv. Opt. Mater.* **2015**, *3*(9), 1201-1206.

(11) Zheng, G.; Mühlenbernd, H.; Kenney, M.; Li, G.; Zentgraf, T.; Zhang, S. Metasurface holograms reaching 80% efficiency. *Nat. Nanotechnol.* **2015**, *10*(4), 308-312.

(12) Wen, D.; Yue, F.; Li, G.; Zheng, G.; Chan, K.; Chen, S.; Chen, M.; Li, K.F.; Wong, P.W.H.; Cheah, K.W.; Pun, E.Y.B. Helicity multiplexed broadband metasurface holograms. *Nat. Commun.* **2015**, *6*, 8241.

(13) Chen, J.; Li, T.; Wang, S.; Zhu, S. 2017. Multiplexed holograms by surface plasmon propagation and polarized scattering. *Nano Lett.* **2017**, *17*(8), 5051-5055.

(14) Lin, J.; Mueller, J. B.; Wang, Q.; Yuan, G.; Antoniou, N.; Yuan, X. C.; Capasso, F. Polarization-controlled tunable directional coupling of surface plasmon polaritons. *Science* **2013**, *340*(6130), 331-334.

(15) Zhang, X.; Xu, Q.; Li, Q.; Xu, Y.; Gu, J.; Tian, Z.; Ouyang, C.; Liu, Y.; Zhang, S.; Zhang, X.; Han, J.; Zhang, W. Asymmetric excitation of surface plasmons by dark mode coupling. *Science Adv.* 2016, *2*(2), 1501142.

(16) Ding, F.; Deshpande, R.; Bozhevolnyi, S. I. Bifunctional gap-plasmon metasurfaces for visible light: polarization-controlled unidirectional surface plasmon excitation and beam steering at normal incidence. *Light: Science & Appl.* 2018, *7*(4), 17178.

(17) Zhang, S.; Genov, D.A.; Wang, Y.; Liu, M.; Zhang, X. Plasmon-induced transparency in metamaterials. *Phys. Rev. Lett.* **2008**, *101*(4), 047401.

- (18) Zhao, Y.; Alù, A. Manipulating light polarization with ultrathin plasmonic metasurfaces. *Phys Rev. B* **2011**, 84(20), 205428.
- (19) Yu, N.; Aieta, F.; Genevet, P.; Kats, M.A.; Gaburro, Z.; Capasso, F. A broadband, background-free quarter-wave plate based on plasmonic metasurfaces. *Nano Lett.* **2012**, 12(12), 6328-6333.
- (20) Park, J.; Kang, J. H.; Kim, S. J.; Liu, X.; Brongersma, M. L. Dynamic reflection phase and polarization control in metasurfaces. *Nano Lett.* **2016**, 17(1), 407-413.
- (21) Huang, L.; Chen, X.; Mühlenbernd, H.; Li, G.; Bai, B.; Tan, Q.; Jin, G.; Zentgraf, T.; Zhang, S. Dispersionless phase discontinuities for controlling light propagation. *Nano Lett.* **2012**, 12(11), 5750-5755.
- (22) Khorasaninejad, M.; Ambrosio, A.; Kanhaiya, P.; Capasso, F. Broadband and chiral binary dielectric meta-holograms. *Science Adv.* **2016**, 2(5), 1501258.
- (23) Wu, P.C.; Tsai, W.Y.; Chen, W.T.; Huang, Y.W.; Chen, T.Y.; Chen, J.W.; Liao, C.Y.; Chu, C.H.; Sun, G.; Tsai, D.P. Versatile polarization generation with an aluminum plasmonic metasurface. *Nano Lett.* **2016**, 17(1), 445-452.
- (24) Lin, D.; Fan, P.; Hasman, E.; Brongersma, M.L. Dielectric gradient metasurface optical elements. *Science* **2014**, 345(6194), 298-302.

(25) Tan, Q.; Guo, Q.; Liu, H.; Huang, X.; Zhang, S. Controlling the plasmonic orbital angular momentum by combining the geometric and dynamic phases. *Nanoscale* **2017**, *9*(15), 4944-4949.

(26) Mueller, J.B.; Rubin, N.A.; Devlin, R.C.; Groever, B.; Capasso, F. Metasurface polarization optics: independent phase control of arbitrary orthogonal states of polarization. *Phys. Rev. Lett.* **2017**, *118*(11), 113901.

(27) Ponsetto, J.L.; Bezryadina, A.; Wei, F.; Onishi, K.; Shen, H.; Huang, E.; Ferrari, L.; Ma, Q.; Zou, Y.; Liu, Z. Experimental demonstration of localized plasmonic structured illumination microscopy. *ACS nano* **2017**, *11*(6), 5344-5350.

(28) Wang, Q.; Bu, J.; Tan, P.S.; Yuan, G.H.; Teng, J.H.; Wang, H.; Yuan, X.C. Subwavelength-sized plasmonic structures for wide-field optical microscopic imaging with super-resolution. *Plasmonics* **2012**, *7*(3), 427-433.

(29) Gustafsson, M. G. Surpassing the lateral resolution limit by a factor of two using structured illumination microscopy. *Journal of microscopy* **2000**, *198*(2), 82-87.

(30) Mudry, E.; Belkebir, K.; Girard, J.; Savatier, J.; Le Moal, E.; Nicoletti, C., Allain, M.; Sentenac, A. Structured illumination microscopy using unknown speckle patterns. *Nat. Photon.* **2012**, *6*(5), 312-315.

(31) Wei, F.; Liu, Z. Plasmonic structured illumination microscopy. *Nano Lett.* **2010**, *10*(7), 2531-2536.

(32) Liang, F.; Jing-Lei, D.; Xiao-Wei, G.; Jing-Quan, W.; Zhi-You, Z.; Xian-Gang, L.; Chun-Lei, D. The theoretic analysis of maskless surface plasmon resonant interference lithography by prism coupling. *Chin. Phys. B* **2008**, *17*(7), 2499.

(33) Sreekanth, K.V.; Murukeshan, V.M. Large-area maskless surface plasmon interference for one-and two-dimensional periodic nanoscale feature patterning. *JOSA A* **2010**, *27*(1), 95-99.

(34) Quidant, R.; Girard, C. Surface-plasmon-based optical manipulation. *Laser & Photon. Rev.* **2008**, *2*(1-2), 47-57.

(35) Spektor, G.; Kilbane, D.; Mahro, A. K.; Frank, B.; Ristok, S.; Gal, L.; Kahl, P.; Podbiel, D.; Mathias, S.; Giessen, H.; Heringdorf, F.; Orenstein, M.; Aeschlimann, M. (2017). Revealing the subfemtosecond dynamics of orbital angular momentum in nanoplasmonic vortices. *Science* **2017**, *355*(6330), 1187-1191.

(36) Huang, J. S.; Callegari, V.; Geisler, P.; Brüning, C.; Kern, J.; Prangma, J. C.; Wu, X.; Feichtner, T.; Ziegler, J.; Weinmann, P.; Kamp, M.; Forchel, A.; Biagioni, P.; Sennhauser, U.; Kamp, M. Atomically flat single-crystalline gold nanostructures for plasmonic nanocircuitry. *Nat. commun.*, **2010**, *1*(1), 1-8.

(37) Liu, Z. Plasmonics and Super-resolution Imaging. *CRC Press* **2017**.

BRIEFS

A polarization tunable structured plasmonic fields (SPF) for subdiffractive imaging is experimentally demonstrated by a fishbone-shaped metasurface on a thin gold film.

SYNOPSIS

Table of Contents

